CHAPTER 3

APPLICATION OF PURE ZnO AND WO_3-DOPED ZnO FOR USE AS PHOTOCATALYSTS

3.1 Introduction

ZnO is an n-type semiconductor that has attracted much attention with respect to the degradation of various pollutants due to its high photosensitivity and stability [1-3]. The photocatalysts is a catalyst which is activated by light irradiation. It adsorbs the energy of the light and transfer the energy to the substances, causing photochemical reaction. While TiO_2 is widely employed as a photocatalyst [4-12], ZnO is a suitable alternative to TiO_2 as it has a similar band gap energy (E_g, 3.2 eV) [13-14], and higher photocatalytic efficiencies was reported [15-20].

3.1.1 Electronic properties of semiconductor [21-24]

ZnO is able to degrade a wide range of stubborn organics and inorganic pollutants due to its ability to generate highly oxidizing and reducing species. This is because as a semiconductor (Sc), it could be "photoexcited" by absorbing light of suitable wavelength to generate two types of electronic carriers, the electrons (e^-) (the reducing species) and holes (h^+) (the oxidizing species) according to equation 3.1

$$Sc \xrightarrow{h\nu > E_g} e^- + h^+ \qquad (3.1)$$

where h is the Planck's constant, v is the frequency of light and hv is the photon energy. To achieve photoexcitation, hv must be greater than E_g, which is known as the optical bandgap of the semiconductor. E_g is defined as the region devoid of energy levels as illustrated in Figure 3.1. For many compounds, as the number N of monomeric units in a particle increases, the energy necessary to photoexcite the

particle decreases. When N is much greater than 2000, a particle which exhibits the band electronic structure of a semiconductor could form. Such a particle would consist of a highest occupied energy band, the valence band (E_{VB}), and the lowest unoccupied energy band, the conduction band (E_{CB}), separated by E_g. Photoexcitation involves the promotion of an e^- from the valence band (E_{VB}) to the conduction band (E_{CB}) upon adsorption of a photon of energy exceeding the band-gap (that is $hv > E_g$) by the semiconductor, simultaneously generating a hole, h^+, in the valence band. A hole can be rationalised as a vacancy devoid of an electron. In general, ZnO has relatively large band gap energy of 3.2 eV as shown in Figure 3.2.

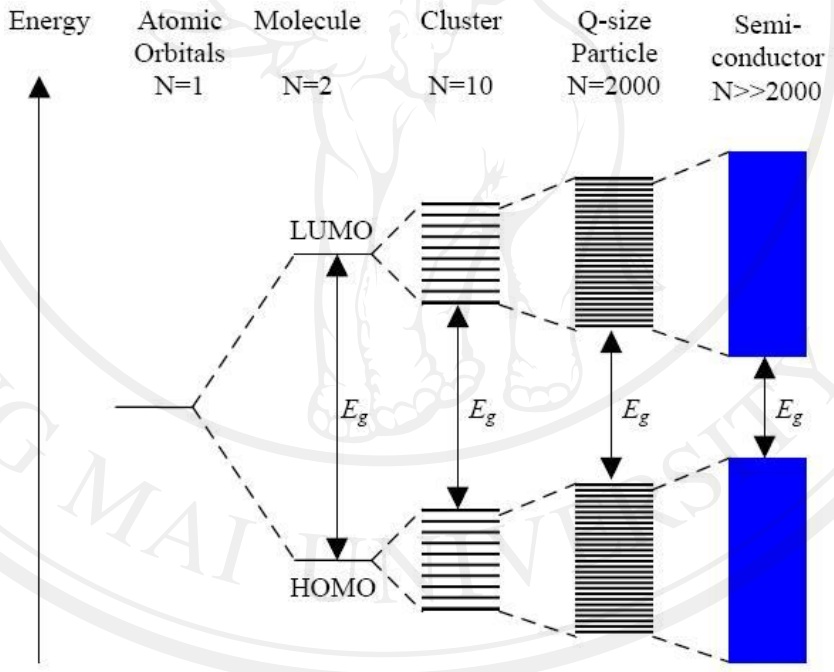

Figure 3.1 The effect of the increase in the number N of monomeric units from unity to cluster of more than 2000 on the electronic structure of a semiconductor compound [22]

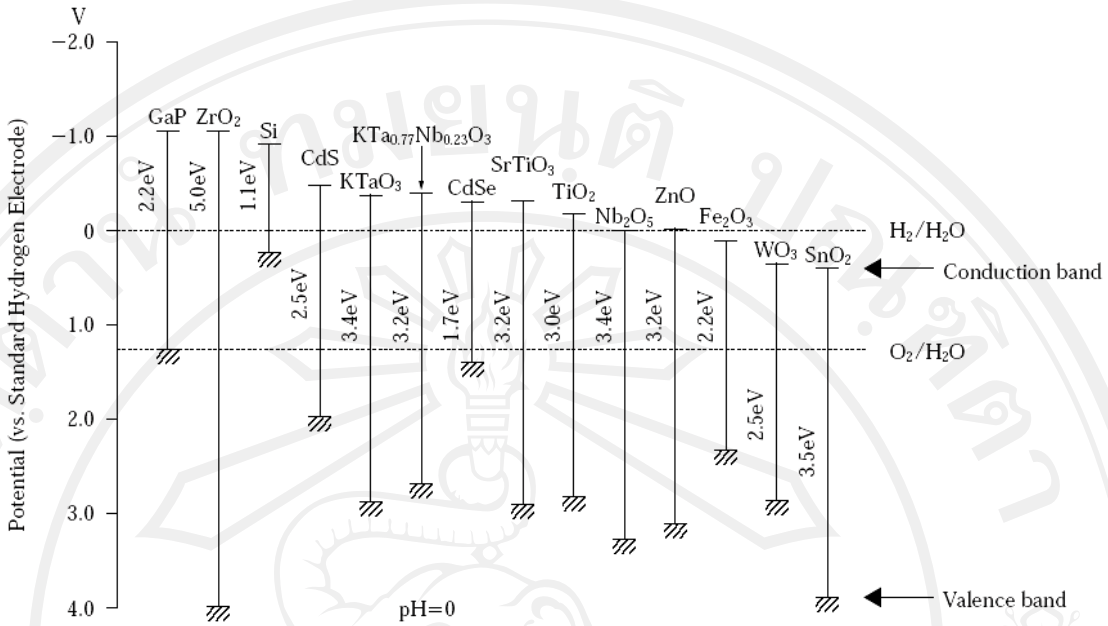

Figure 3.2 Energy structures of various photosemiconductors [23]

3.1.2 Mechanistic of ZnO Semiconductor Photocatalysis [21-26]

The photoelectrochemistry of the n-type ZnO semiconductor in contact with an electrolyte is depicted in Figure 3.3. When the ZnO particles are brought into contact with an electrolyte, the excess charge carriers (e^-) are transferred from the ZnO surface to the electrolyte in order to equilibrate the Fermi levels of the ZnO and the electrolyte. This leads to band-bending and the formation of a thin-layer of space charge region, normally a few Angstroms in width on the surface of the ZnO. For ZnO particles of sizes greater than 10 nm, the space charge layer formed on the planar electrodes must be formed in the surface region of the particles. This layer is called the depletion layer as the majority charge carriers are depleted into the electrolyte. This region is positively charged as the excess electrons on the surface are being transferred to the electrolyte, hence resulting in an electric field directed from the ZnO surface (positively-charged) to the electrolyte.

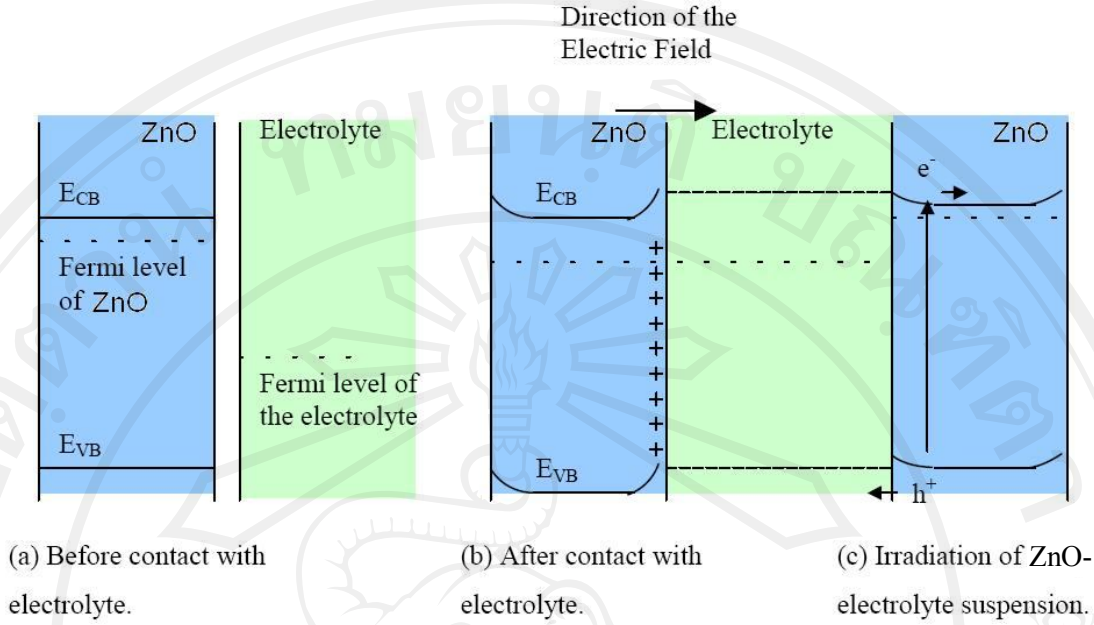

Figure 3.3 Illustrations of electrochemistry of ZnO particles in contact with an electrolyte and after irradiation. (a) Fermi level near the conduction band in ZnO prior to contact with an electrolyte. (b) Band-bending and the presence of an electric field after contact with electrolyte. (c) Transfer of the photogenerated electrons and holes upon irradiation. E_{VB}: Valence band, E_{CB}: Conduction band [21].

When the e^- and h^+ are generated following irradiation, they can take part in processes as illustrated in Figure 3.4. The e^--h^+ recombination can occur in the bulk (reaction 1a) and/or on the surface (reaction 1b). When the h^+ and e^- are successfully transferred to the ZnO surface, the h^+ can oxidize an electron donor D such as H_2O (reaction 2a) while the e^- can reduce an electron acceptor (O_2, reaction 2b). The redox reactions 2a and 2b are desirable as they lead to the destruction of organics and inorganic pollutants via oxidation and reduction processes respectively. These processes are believed to occur mainly on the ZnO surface. The presence of the species H_2O and O_2 on the ZnO surface is hence imperative to the capture of h^+ and e^-

respectively. Species D could be a surface hydroxyl group or an adsorbed organic molecule.

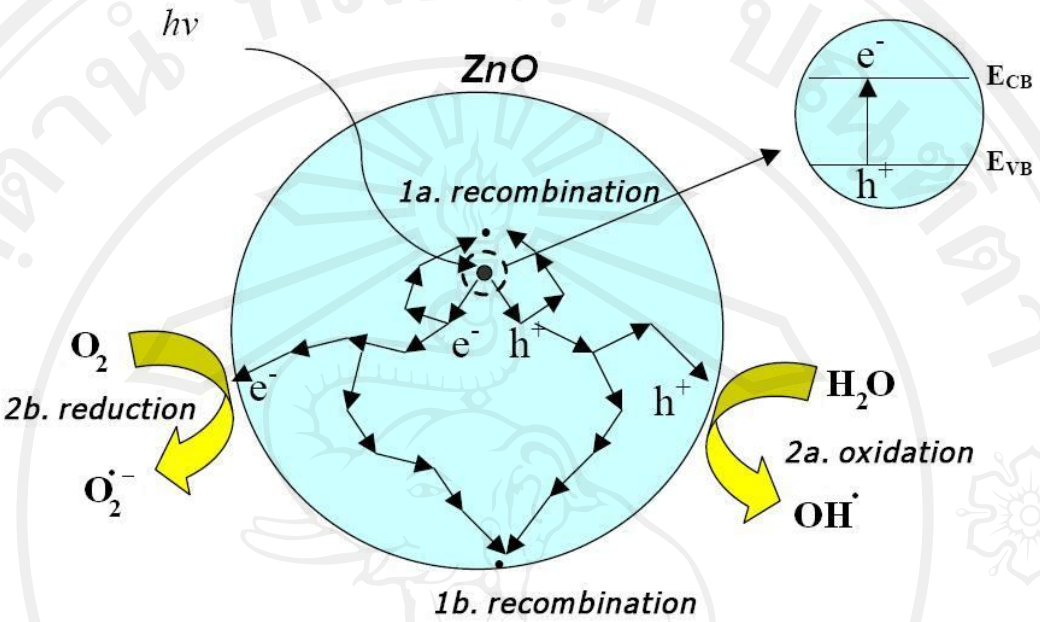

Figure 3. 4 The possible pathways of the main charge carriers occurring in a ZnO particle following photoexcitation. E_{VB}: Valence band, E_{CB}: Conduction band [21].

To summarize the reactions depicted in Figure 3.4, the major processes in ZnO photocatalysis can be generalized by the following set of simplified equations (Equation 3.2-3.9). Because it was established that the photocatalysed degradation of organic matter in solution was initiated by photoexcitation of the semiconductor, followed by the formation of an electron–hole pair on the surface of catalyst (Equation 3.2). The high oxidative potential of the hole (h^+_{VB}) in the catalyst permits the direct oxidation of organic matter (methanol, glucose and sucrose) to reactive intermediates (Equation 3.3). Very reactive hydroxyl radicals can also be formed either by the decomposition of water (Equation 3.4) or by the reaction of the hole with OH^- (Equation 3.5). The hydroxyl radical is an extremely strong, non-selective

oxidant which leads to the partial or complete mineralization of several organic chemicals [27].

$$ZnO + h\nu \rightarrow ZnO\ (e^-_{CB} + h^+_{VB}) \quad (3.2)$$

$$h^+_{VB} + \text{organic} \rightarrow \text{organic}^{\bullet+} \rightarrow \text{oxidation of the organic} \quad (3.3)$$

$$h^+_{VB} + H_2O \rightarrow H^+ + OH^\bullet \quad (3.4)$$

$$h^+_{VB} + OH^- \rightarrow OH^\bullet \quad (3.5)$$

Electron in the conduction band (e^-_{CB}) on the catalyst surface can reduce molecular oxygen to superoxide anion (Equation 3.6). This radical, in the presence of organic scavengers, may form organic peroxides (Equation 3.7) or hydrogen peroxide (Equation 3.8).

$$e^-_{CB} + O_2 \rightarrow O^{\bullet}_2{}^- \quad (3.6)$$

$$O^{\bullet}_2{}^- + \text{organic} \rightarrow \text{organic} - OO^\bullet \quad (3.7)$$

$$O^{\bullet}_2{}^- + HO_2^\bullet + H^+ \rightarrow H_2O_2 + O_2 \quad (3.8)$$

Electrons in the conduction band are also responsible for the production of hydroxyl radicals, species which have been indicated as the primary cause of organic matter degradation (Equation 3.9).

$$OH^\bullet + \text{organic} \rightarrow \text{degradation of organic} \quad (3.9)$$

The overall degradation organic compound process in the presence of oxygen can be summarized by the following Equation 3.10 [21].

$$C_mH_nO_yX_z + (m + \frac{sz}{2} - \frac{kz}{4} - \frac{y}{2})O_2 \xrightarrow{ZnO,\, h\nu \geq E_{bg}} mCO_2 + \frac{n-kz}{2}H_2O + kzH^+ + zXO_s^{-k} \quad (3.10)$$

3.1.3 Photocatalytic oxidation

The photooxidation of organic compounds has been interested for many environmental applications such as waste water pollutant treatments. Many kinds of organic compounds have been reported to be degraded by photocatalytic process. The photooxidation of organic compounds proceeds via hydroxyl radical or directly by the photogenerated holes. Evidence that the hydroxyl radical is the main reactive oxidant in the photocatalytic degradation has been obtained by observing the intermediates of the photooxidation of halogenated aromatic compounds which are the same as those when these compounds were reacted with a known source of hydroxyl radicals [28].

3.1.4 Photocatalytic reduction

Photogenerated electrons at the conduction band of ZnO are relatively weaker reductants. However, the presence added electron donor as organic hole scavenger is important in photocatalytic reduction process because it can be enhanced the reaction. In addition, hole scavengers, or some organic compounds could form reducing intermediates upon reacting with the hydroxyl radicals which could enhance the reduction reactions [29].

3.1.5 Modified photocatalysts: enhancement of photocatalytic activity

Interfacial charge transfer in the reactions when occurs could enhance the photoactivity. Improved charge separation and inhibition of charge carrier recombination is essential in improving the overall quantum efficiency for interfacial charge transfer. This can be achieved by modifying the properties of the particles by a selective surface treatment.

3.1.5.1 Doping with transition metal ions [25-26]

The performance of photocatalysts can be changed by doping the transition metal ions into ZnO particles. The dynamics of electron-hole recombination and interfacial charge transfer will be affected. While some studies have shown that doping with transition metal ion into ZnO semiconductors can be effective in lengthening the lifetime of the generated charge carriers. Several reasons in the research papers explained the effects of the dopant on ZnO. One reason is that the location and co-ordination of the dopant within the semiconductor. This depends critically on the sample preparation techniques, pretreatment, and the concentration of the dopant. The dopant may be adsorbed on the surface, or incorporated into the interior of the particle upon firing, or they may form separate oxide phases. The dopant can function as both hole and electron trap or they can mediate interfacial charge transfer. Once incorporated into the interior of ZnO, the dopant may occupy either lattice substitutional or interstitial sites. Their ability to function as trap site and/or to mediate interfacial charge transfer will depend on these factors. Finally, the site where the electron gets trap greatly influences the redox chemistry of the doped semiconductor. However, if an electron is trapped in a deep trapping site, it will have a longer lifetime, but it may also have a lower redox potential. This might result in a decrease in the photoreactivity.

3.1.5.2 Metal ion deposition [21, 25-26]

The ability of a metal that is deposited on semiconductor surface to mediate the photogenerated electrons away from the semiconductor may give rise to a Schottky barrier. A Schottky barrier is created at a metal-semiconductor interface. The potential barrier formed at the interface depends on the work functions of the two

materials. The work function (Φ) is defined as the energy difference between the vacuum level (E_{vac}) and the Fermi level (E_F). The E_{vac} is defined as the energy of an electron at rest (and hence with zero kinetic energy) just outside the crystal surface and not interacting with the crystal. When the metal and semiconductor are brought into intimate contact, electron flow from the semiconductor to the metal until the Fermi level on both side are equalized. The transfer of electrons could be rationalized as follows: the energy barrier for the electron transfer from a region of higher work function (metal ions) to one of lower work function semiconductor (ZnO) is greater than that from a lower work function to one the higher work function.

3.1.5.3 Semiconductor compound deposition [21, 25-26]

Semiconductor compound deposition on the surface of the photocatalyst is also utilized enhance the separation of electron-hole pairs. When semiconductor compound deposition on photocatalyst, it can change the photocatalyst surface properties. Figure 3.5 illustrates the WO_3 in contact with surface of semiconductor. Upon excitation, electron can migrate to the WO_3 deposit where they can be trapped or captured by an oxidant (O_2-electron acceptor). The hole is then free to migrate to the surface where oxidation can be occur ($H_2O \rightarrow OH^{\bullet}$).

In a coupled semiconductor system the two particles are in contact with each other and both holes and electrons are accessible on the surface for selective oxidation and reduction processes. The possessing different energy levels for their corresponding conduction and valence bands, provides an approach to achieve a more efficient charge separation, an increased lifetime of the charge carriers and an enhanced interfacial charge transfer to adsorbed substrates. An interesting approach to prevent electron-hole recombination is the coupling of two semiconductor catalyst

to improve charge separation. This strategy accomplishes vector displacement of charges on the semiconductors and reduces electron-hole recombination. Thus, coupled semiconductor systems offer potential advantages for solar energy utilization because of the possibilities presented by inter-particle electron transfer.

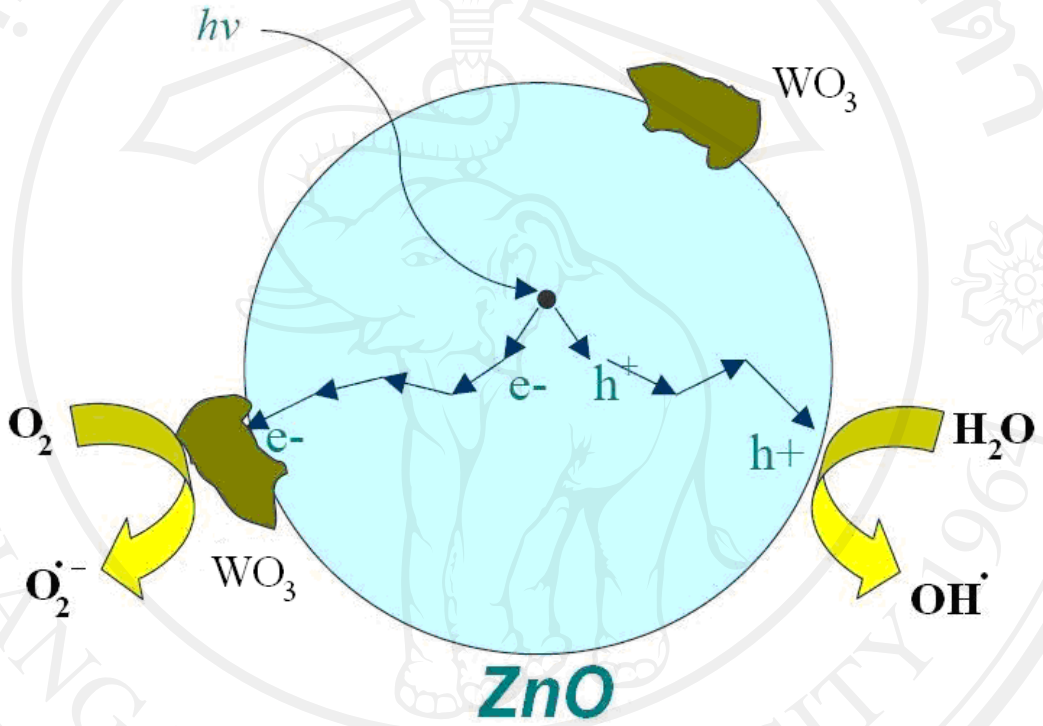

Figure 3.5 Electron mediation by WO_3 in contact with ZnO surface [21]

3.1.6 Literature review

The photocatalytic decolorization of Reactive Blue 19 (RB-19) in aqueous solutions containing TiO_2 or ZnO as the catalysts was reported by Lizama et al. [15]. Titania P-25 (surface area 50 $m^2\ g^{-1}$) was obtained from Degussa and ZnO (surface area 5 $m^2\ g^{-1}$) from Merck. It was noticed that ZnO was a more efficient catalyst than TiO_2 in the color removal of RB-19.

The degradation of acid 14, commonly used as a textile dye, using ZnO as photocatalyst was reported by Daneshvar et al. [16]. It was found that ZnO was a suitable alternative to TiO_2 for the degradation of this dye, since its photodegradation mechanism was proven to be similar to that of TiO_2.

The photocatalytic degradation of Methyl Orange (MO) and Rhodamine 6G (R6G) in various photocatalyst suspensions (TiO_2, ZnO, SnO_2, ZnS and CdS) was investigated by Kansal et al. [20]. It was found that the most active photocatalyst for decolorization of MO and R6G was ZnO. The initial rate of photodecolorization increased with increase in catalyst dose up to an optimum loading. Further increase in catalyst dose showed no effect. Moreover, photocatalytic activity of ZnO is greater in the presence of solar light as compared to UV light.

Metal and metal oxide such as Ag, Pd, Fe, Cd and W had been shown to have a beneficial influence on the photoactivity of nanocrystalline semiconductor photocatalysts. The photocatalytic degradation of phenol solution using ZnO nanoparticles that were modified by depositing different amount of noble metal Ag or Pd on their surfaces with a photoreduction method was reported by Liqiang et al. [30]. The results show that the photocatalytic activity of ZnO nanoparticles was greatly improved by these noble metals. Moreover, the effects of Pd modification on photocatalytic activity are greater than that of Ag.

The photocatalytic activities of α-Fe_2O_3, WO_3 and CdS deposited on ZnO on dichloro acetic acid (DCA) in aqueous solution were investigated by Sakthivel et al. [31]. The results reveal that the mixtures of ZnO with α-Fe_2O_3 (0.5 wt.%), WO_3 (0.02 wt.%) and CdS (0.2 wt.%) exhibit higher photocatalytic activity than pure ZnO when the experiments were carried out using all the three conditions such as (1) under continuous purging with molecular oxygen, (2) in the presence of naturally dissolved

oxygen and (3) in the absence of oxygen. Moreover, it can be concluded that the main role of α-Fe_2O_3, WO_3 and CdS as heterojunctions, is the improved separation of photoproduced electron/hole pairs and, consequently, results in the observed higher photocatalytic activity.

The size of photocatalyst is one of the most important factors. Hariharan [2] compared the photocatalytic activity between bunk ZnO and ZnO nanoparticles, the results indicated that ZnO nanoparticles exhibited higher activity than bunk ZnO. Moreover, the photocatalyst preparation process is another important factor. Wang et al. [32] compared photocatalytic activity of ZnO powder with various size scales (mean diameter size: 10, 50, 200 and 1000 nm) preparing by two different preparation processes as thermal evaporation process and chemical deposition process. ZnO nanoparticles with diameter size 50 nm prepared by thermal evaporation process showed the highest photocatalytic activity. However, the smaller 10 nm ZnO nanoparticles prepared by chemical deposition process showed the lower efficiency contrast to 200 nm ZnO powders prepared by thermal evaporation process, indicating that preparation process was the decisive factor rather than size and morphology.

The photocatalytic degradation of 10 ppm methylene blue (MB) solution that was used to evaluate the performance of FSP-made Ag-ZnO and compared to wet-made Ag-ZnO was reported by Height et al. [33]. The results showed that the photocatalytic activity of FSP-made Ag-ZnO was much better than that of wet-made Ag-ZnO. Moreover, FSP-made 3 at% Ag-loaded ZnO exhibited the best photocatalytic performance. This result could be confirmed that the preparation process is very important factor for photocatalysts.

3.2 Experimental

3.2.1 Apparatus

- Spiral photoreactor (Nanoscience Research Laboratory, Faculty of Science, Chiang Mai University (CMU), Thailand)
- UV-lamp (NEC 20 watt T10 black light blue)
- Peristaltic pump (Masterflex Model 7553-79)
- Conductivity meter (EUTECH PC 5500)

In this work, pure ZnO and WO_3-doped ZnO nanoparticles prepared by FSP method were tested for photocatalytic activity by using the setup of spiral photoreactor at Nanoscience Research Laboratory, Faculty of Science, Chiang Mai University (CMU), Thailand. A schematic diagram of the spiral photoreactor was given in Figure 3.6. The spiral photoreactor consisted of (I) 70 cm long spiral reactor. The spiral reactor was made out of borosilicate glass tube with an outside diameter of 5 mm and the wall thickness of 1 mm. Photocatalytic reaction was initiated by illuminating the suspension which suspended inside the tube with (II) UV-lamp (NEC 20 watt T10 black light blue). The glass spiral filtered with the lamp was covered with aluminum foil to prevent both the intrusions of ambient light and the emission of the harmful UV from the lamp. The attachment to the photoreactor were (III) a peristaltic pump (Masterflex Model 7553-79) (IV) a conductivity meter EUTECH PC 5500 and (V) a gas-liquid separator. All components were connected together using masterflex flexible tubing which was resistant to leaching of any organics.

3.2.2 Preparation of photocatalyst suspension and operation

A 50 mL suspension of pure ZnO and WO_3-doped ZnO nanoparticles having a loading of 1 g/L was prepared and its pH was about 7.0. The suspension was dispersed in an ultrasonic bath for 20 min before it was discharged into the spiral photoreactor. The suspension was circulated through out the spiral photoreactor. The suspension was subjected to a "carbon burn off" period, when it was illuminated to remove any contaminants adsorbed on the photocatalyst surface. The carbon dioxide generation was monitored using the conductivity meter (IV) in unit μS/cm. During carbon burn off, the conductivity reading increased to a constant value which was an indicating or that all impurities were removed. The system was then slowed to equilibrate at ambient atmospheric conditions by opening a valve at an exit port of a gas liquid separator (V).

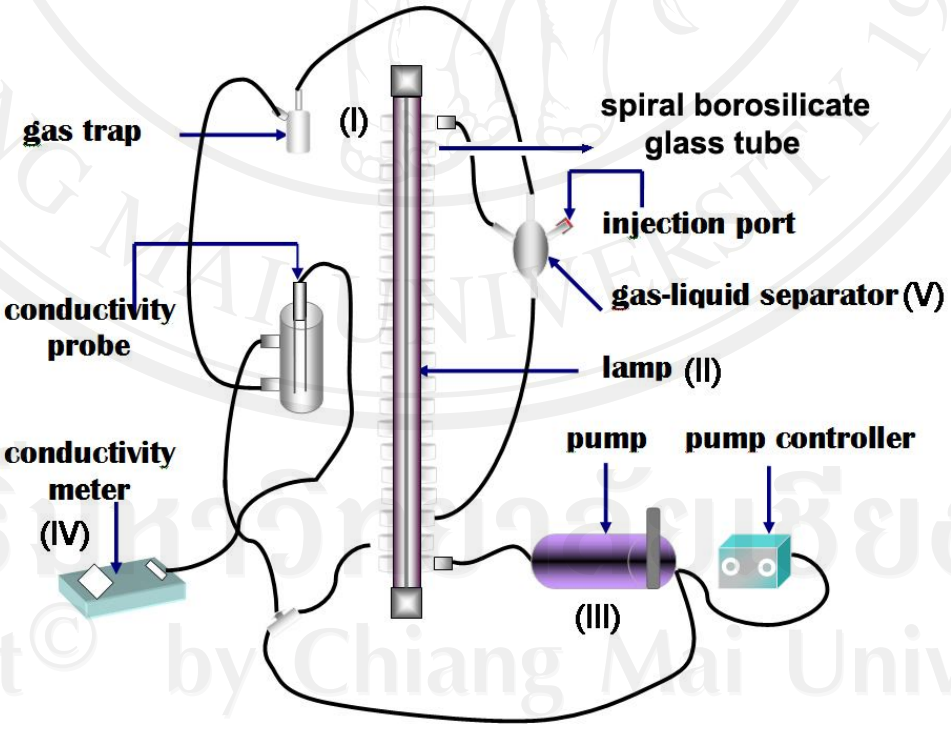

Figure 3.6 Scheme of spiral photoreactor

Various organic carbon load (500 μg of carbon (500 μg C)), as glucose, sucrose and methanol were injected into photocatalyst suspension through the inlet port (V). The catalyst-organic substrate mixture was circulated for 5 min without light illumination to ensure dispersion of the organic compound throughout the slurry. The lamp was then switched on. Subsequently, the increase in conductivity value was recorded every 1 second until the reaction ended. At the end of the photoreaction, the lamp was switched off and the system was flushed several times with Milli-Q water. All experiments were repeated at least twice.

3.2.2.1 Calibration curve measurement

The spiral photoreactor was calibrated to obtain a relationship between the conductivity value and the amount of degraded organics. A suspension of pure ZnO as a catalyst loading (1 g/L) was used during the calibration. The photocatalyst was circulated through the reactor and subjected to carbon burn off. After carbon burn-off, a known amount of carbon was added as sucrose (100-2000 μg of carbon) to the system and the lamp switched on. The conductivity value increased and the final conductivity reading was recorded as in the previous section which, corresponding to the known amount of carbon added. Calibration was relied on the establishing of the relation between carbon mass in the sample and the conductivity measurement values.

For calculation, at the end of each run the recorded data which consisted of the increased in conductivity value was converted to the amount of carbon interpolated from the expression obtained from the calibration curve.

3.3 Results and discussion

3.3.1 The methanol degradation curve

The percent of degradation of methanol as a function of time using pure and WO_3-doped ZnO nanoparticles photocatalyst containing 0.25, 0.50, 0.75 and 1.0 mol% WO_3 were shown in Figure 3.7. All curves of methanol degradation with different concentrations of WO_3 in ZnO photocatalyst looked similar to "S" character. Each curve could be divided to 4 periods. The first period was in the range of 0-15 min and 0-25 min when WO_3-doped ZnO and pure ZnO were used as photocatalysts, respectively. The methanol was slowly degraded and the slope was quite low. The second period was in the range of 15-20 min and 25-35 min when WO_3-doped ZnO and pure ZnO were used as photocatalysts, respectively. The percent of methanol degradation greatly increased and the slope was very high. The third period was in the range of 20-30 min and 35-45 min when WO_3-doped ZnO and pure ZnO were used as photocatalysts, respectively. The methanol degradation was slightly processed and the slope was quite low again. The forth period was after 46, 32, 28, 35 and 35 min for pure and WO_3-doped ZnO nanoparticle photocatalysts containing 0.25, 0.50, 0.75 and 1.0 mol% WO_3, respectively when the curve changed a little in this period then the methanol degradation process was completed.

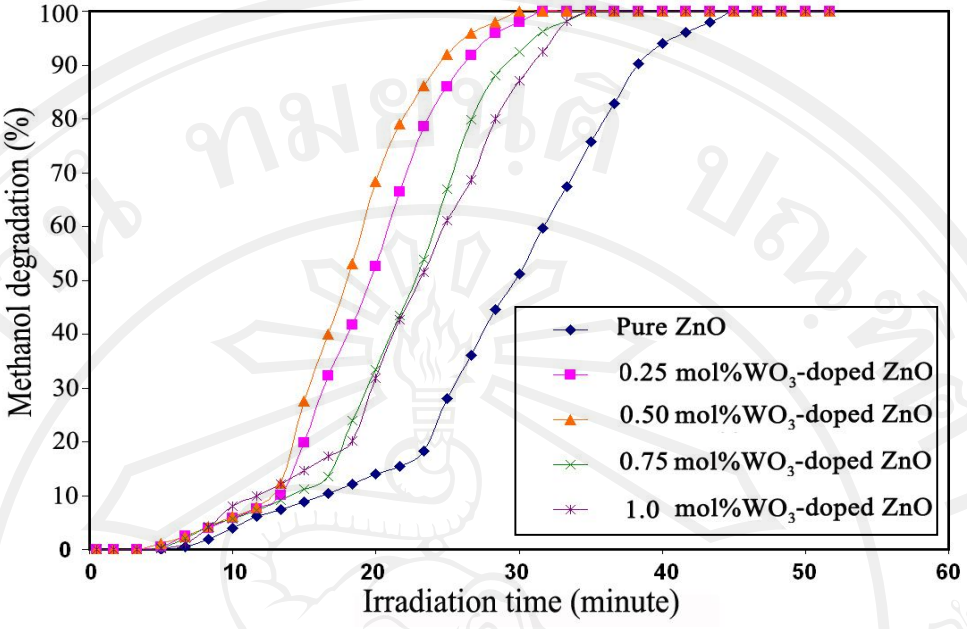

Figure 3.7 The percent of degradation of methanol using pure and WO_3-doped ZnO nanoparticles photocatalyst containing 0.25, 0.50, 0.75 and 1.0 mol%WO_3

3.3.2 The glucose degradation curve

The percent of degradation of glucose as a function of time using pure and WO_3-doped ZnO nanoparticles photocatalyst containing 0.25, 0.50, 0.75 and 1.0 mol% WO_3 were shown in Figure 3.8. All curves of glucose degradation with different concentrations of WO_3 in ZnO photocatalyst looked similar to "S" character. Each curve could be divided to 4 periods. The first period was in the range of 0-20 min when the glucose degradation was slightly processed and the slope was low. The second period was in the range of 20-35 min when the percent of glucose degradation greatly increased and the slope was very high. The third period was in the range of 35-45 min when the glucose degradation was slightly processed, the slope was low again. The forth period was after 58, 46.5, 46, 58 and 60 min for pure and WO_3-doped ZnO nanoparticles photocatalyst containing 0.25, 0.50, 0.75 and 1.0 mol% WO_3,

respectively when the curve changed a little in this period then the glucose degradation process was completed.

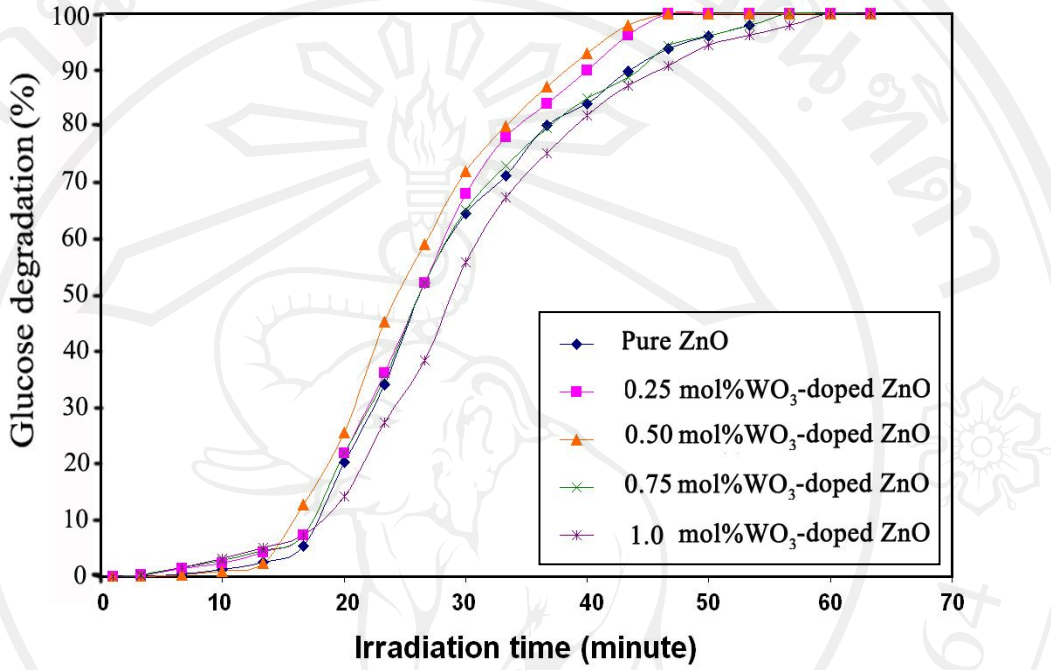

Figure 3.8 The percent of degradation of glucose using pure and WO_3-doped ZnO nanoparticles photocatalyst containing 0.25, 0.50, 0.75 and 1.0 mol%WO_3

3.3.3 The sucrose degradation curve

The percent of degradation of sucrose as a function of time using pure and WO_3-doped ZnO nanoparticles photocatalyst containing 0.25, 0.50, 0.75 and 1.0 mol% WO_3 were shown in Figure 3.9. All curves of sucrose degradation with different concentrations of WO_3 in ZnO photocatalyst looked similar to "S" character. Each curve could be divided to 4 periods. The first period was in the range of 0-20 min when the sucrose degradation was slightly processed and the slope was quite low. The second period was in the range of 20-32 min when the percent of sucrose degradation greatly increased and the slope was very high. The third period was in the

range of 32-45 min when the sucrose degradation was slightly processed and the slope was low again. The forth period was after 56, 48, 47, 50 and 55 min for pure and WO_3-doped ZnO nanoparticles photocatalyst containing 0.25, 0.50, 0.75 and 1.0 mol% WO_3, respectively when the curve changed a little in this period then the sucrose degradation process was completed.

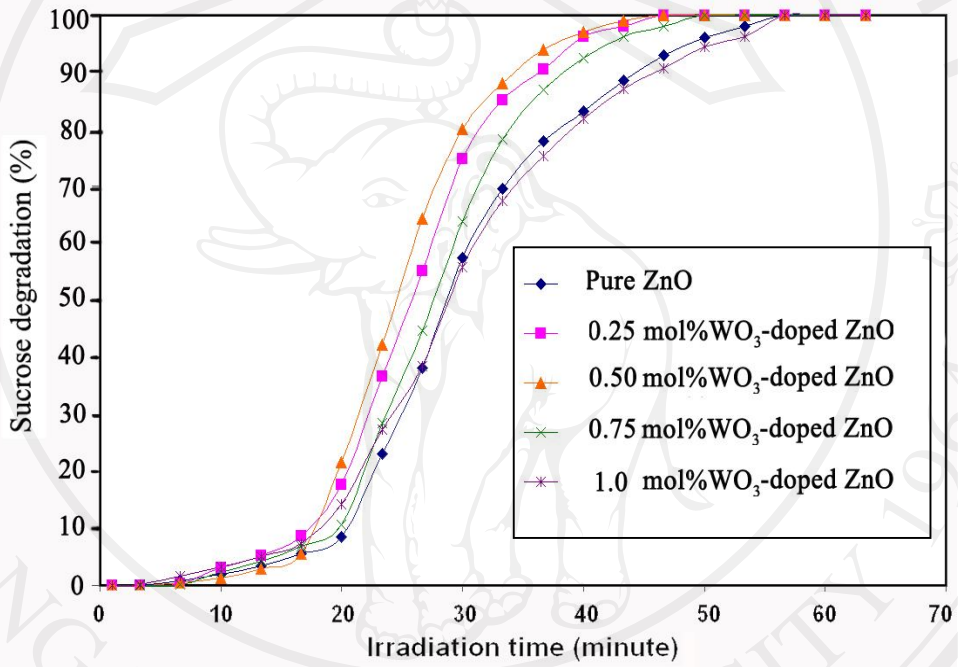

Figure 3.9 The percent of degradation of sucrose using pure and WO_3-doped ZnO nanoparticles photocatalyst containing 0.25, 0.50, 0.75 and 1.0 mol%WO_3

3.3.4 Photocatalytic activity of pure ZnO and WO_3-doped ZnO with methanol, glucose and sucrose under UV irradiation

The activity of ZnO samples can be evaluated by the photocatalytic oxidation reaction of methanol, glucose and sucrose under UV irradiation. It is well known that good photocatalyst takes short time to complete the degradation process. The results from Figure 3.7 show that, 46, 32, 28, 35 and 36 min were spent by the pure and

WO_3-doped ZnO nanoparticles containing 0.25, 0.50, 0.75 and 1.0 mol% WO_3, respectively, as photocatalysts to complete methanol degradation process.

The results from Figure 3.8 show that, 58, 46.5, 46, 58 and 60 min were spent by the pure and WO_3-doped ZnO nanoparticles containing 0.25, 0.50, 0.75 and 1.0 mol% WO_3, respectively, as photocatalysts to complete glucose degradation process. The results from Figure 3.9 show that, 56, 48, 47, 50 and 55 min were spent by the pure and WO_3-doped ZnO nanoparticles containing 0.25, 0.50, 0.75 and 1.0 mol% WO_3, respectively, as photocatalysts to complete sucrose degradation process. The times for completing the degradation process of methanol, glucose and sucrose with different types of photocatalyst could be concluded in Table 3.1.

Table 3.1 The comparison of time for completing the degradation process of methanol, glucose and sucrose with different types of photocatalyst

Photocatalyst type	Completed methanol degradation time (min)	Completed glucose degradation time (min)	Completed sucrose degradation time (min)
None	60	70	70
Pure ZnO	46	58	56
0.25 mol% WO_3-doped ZnO	32	46.5	48
0.50 mol% WO_3-doped ZnO	28	46	47
0.75 mol% WO_3-doped ZnO	35	58	50
1.0 mol% WO_3-doped ZnO	36	60	55

Moreover, it was found that 60, 70 and 70 min were spent by the methanol, glucose and sucrose in the absence of the photocatalyst to finish the degradation process under UV irradiation, indicating that the direct photolysis of methanol, glucose and sucrose could occur in experimental condition but took a longer period of time.

In addition, all WO_3-doped ZnO nanoparticles took shorter time than the pure ZnO to complete methanol, glucose and sucrose degradation process. The 0.50 mol% WO_3-doped ZnO nanoparticles took the shortest time to complete the process. These results could be assumed that the photocatalytic activity of ZnO nanoparticles could be greatly improved by doping an appropriate amount of WO_3. The optimal amount of WO_3 doping into ZnO nanoparticles was 0.50 mol% in methanol, glucose and sucrose. A limiting factor of the photocatalytic reaction should be the recombination of the electron and hole prior to the superoxide activation step.

Figure 3.10 shows the effect of WO_3 loading on the photocatalytic activity of ZnO nanoparticles. It can be seen that the optimized amount of WO_3 loading is 0.50 mol% for methanol, glucose and sucrose degradation. This is consistent with WO_3 particles acting to trap photo-induced electrons, retarding the electron–hole recombination process, and thereby, promoting the photocatalytic activity. If the amount of WO_3 loading is larger than its optimized value, the activity of ZnO nanoparticles begins to go down inversely. One explanation is that an appropriate amount of WO_3 load may become the center for trapping photoelectrons, while an excess amount of WO_3 load may become the center for recombining photoinduced electron and hole pairs [25, 30].

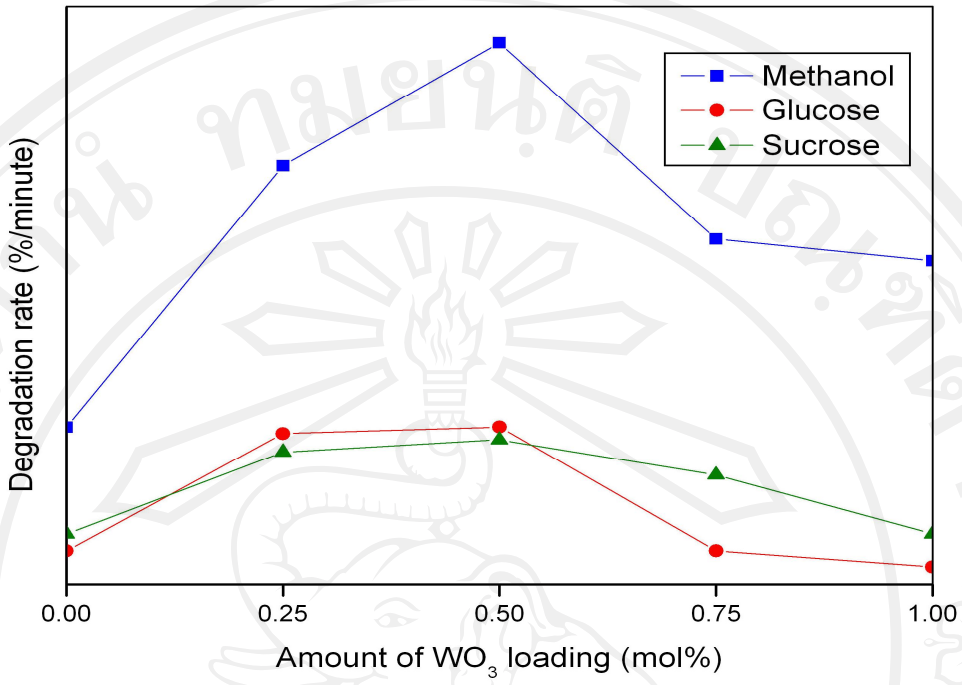

Figure 3.10 Photocatalytic degradation rate of methanol, glucose and sucrose as a function of WO_3 loading on ZnO photocatalyst

Figure 3.11 shows the electronic energy level of O_2 (gas), conduction band (CB) of WO_3 molecular clusters ([*WO*$_3$]n), CB of ZnO, O_2 adsorbed on ZnO surfaces (O_A), WO_3 (bulk) and valence band (VB) of ZnO. The electronic energy level of [*WO*$_3$]n can change to a certain degree with changing WO_3 amount due to the quantum size effect, namely, the lower the WO_3 amount, the higher the electronic energy level. Thus, the direction of the electrons easily transferring to could be determined according to Figure 3.11. The arrowheads of solid line indicated that the electrons could transfer to the direction, while that of dashed line indicated that the electrons could not move to that direction.

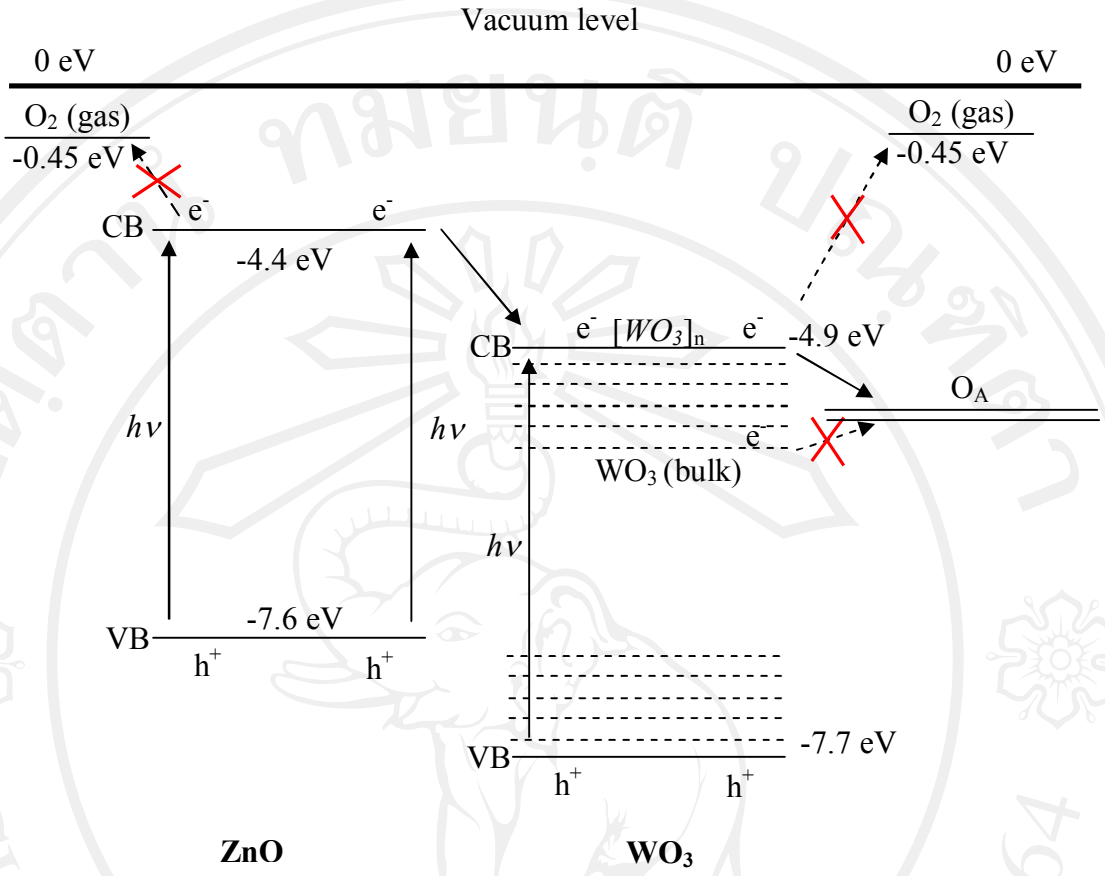

Figure 3.11 Simplified diagram of electronic energy level of conduction (CB) and valance (VB) band of ZnO, electronic energy level of WO_3 clusters ([WO_3]n), WO_3 (bulk) and O_2 adsorbed on ZnO surfaces (O_A) [25, 26, 30].

There were main three results as following: (i) the photoinduced electrons could not transfer directly from the CB of ZnO to O_2 (gas) or indirectly from the CB of ZnO to O_2 (gas) via the CB of WO_3 (bulk); (ii) if the electronic energy level of CB of [WO_3]n was lower than that of the CB of ZnO and higher than that of O_A because of the appropriate content of deposited WO_3, the O_A can easily capture the photoinduced electrons to produce $O_2^{\bullet}$ via CB of [WO_3]n. This is favorable for photocatalytic reactions and the activity of semiconductor photocatalyst was improved by increasing the separation efficiency of photoinduced electron-hole pairs

and by promoting the formation of O_A. (iii) if too much amount of WO_3 is deposited, the electronic energy level of [WO_3]n will decline to or even lower than that of the O_A. Thus, it is difficult for O_A to capture the photoinduced electrons via bulk WO_3, and the photoinduced electron and hole pairs on deposited WO_3 will easily recombine which make the photocatalytic performance decrease. These discussions can be confirmed that the appropriate amount of deposited WO_3 can promote the O_A capturing photoinduced electrons. Moreover, it can be suggested that the separation rate of photoinduced electron and hole pairs and photocatalytic performance of ZnO photocatalyst can be improved by the appropriate amount of deposited WO_3.

3.4 Conclusions

The photocatalytic activity of WO_3-doped ZnO nanoparticles containing 0.25, 0.50, 0.75 and 1.0 mol% were investigated by UV-induced degradation of methanol, glucose and sucrose in aqueous solution in the photocatalytic reactor. The results showed that the appropriate amount of WO_3 loading could greatly enhance the photocatalytic activity of ZnO nanoparticles for degrading methanol, glucose and sucrose. The optimized amount of WO_3 loading was 0.50 mol% in methanol, glucose and sucrose. This is consistent with WO_3 particles acting to trap photoinduced electrons, retarding the electron–hole recombination process, and thereby, promoting the photocatalytic activity.

REFERENCES

1. Byrappa K., Subramani A.K., Ananda S., Lokanatharai K.M., Sunitha M.H., Basavalingu B., Soga K. Impregnation of ZnO onto activated carbon under hydrothermal conditions and its photocatalytic properties. *J. Mater. Sci.*, 2006, **41**, 1355-1362.
2. Hariharan C. Photocatalytic degradation of organic contaminants in water by ZnO nanoparticles. *Appl. Catal., A-Gen.*, 2006; 304: 55-61.
3. Hong R., Pan T., Qian J., Li H. Synthesis and surface modification of ZnO nanoparticles. *Chem. Eng. J.*, 2006, **119**, 71-81.
4. Zhang F., Zhao J., Zang L., Shen T., Hidaka H., Pelizzetti E., Serpone N. Photoassisted degradation of dye pollutants in aqueous TiO_2 dispersions under irradiation by visible light. *J. Mol. Catal. A-Chem.*, 1997, **120**, 173-178.
5. Gonqalves M.S.T., Oliveira-Campos A.M.F., Pinto E.M.M.S., Plasência P.M.S., Queiroz, M.J.R.P. Photochemical Treatment of Solutions of Azo Dyes Containing TiO_2. *Chemosphere*, 1999, **39**, 781-786.
6. Chen J., Liu M., Zhang J., Ying X., Jin L. Photocatalytic degradation of organic wastes by electrochemically assisted TiO_2 photocatalytic system. *J. Environ. Manage.*, 2004, **70**, 43–47.
7. Hasnat M.A., Siddiquey I.A., Nuruddin A. Comparative photocatalytic studies of degradation of a cationic and an anionic dye. *Dyes Pigments*, 2005, **66**, 185-188.

8. Černigoj U., Štangar U.L., Trebše P., Krašovec U.O., Gross S. Photocatalytically active TiO_2 thin films produced by surfactant-assisted sol–gel processing. *Thin Solid Films*, 2006, **495**, 327 – 332.

9. Kusvurana E., Samilb A, Atanura O.M., Erbatur O. Photocatalytic degradation kinetics of di- and tri-substituted phenolic compounds in aqueous solution by TiO_2/UV. *Appl. Catal. B-Environ.*, 2005, **58**, 211-216.

10. Yu H., Zhang K., Rossi C. Theoretical study on photocatalytic oxidation of VOCs using nano-TiO_2 photocatalyst. *J. Photoch. Photobiol. A.,* 2007, **188**, 65-83.

11. Caliman A.F., Cojocaru C., Antoniadis A., Poulios I. Optimized photocatalytic degradation of Alcian Blue 8 GX in the presence of TiO_2 suspensions. *J. Hazard. Mater.*, 2007, **144**, 265-273.

12. Khodja A.A., Sehili T., Pilichowski J.F., Boule P. Photocatalytic degradation of 2-phenylphenol on TiO_2 and ZnO in aqueous suspensions. *J. Photoch. Photobiol. A*, 2001, **141**, 231-239.

13. Sakthivela S., Neppolianb B., Shankarb M.V., Arabindoob B., Palanichamyb M., Murugesan V. Solar photocatalytic degradation of azo dye:comparison of photocatalytic efficiency of ZnO and TiO_2. *Sol. Energ. Mat. Sol. C.*, 2003, **77**, 65-82.

14. Hao Y., Yang M., Li W., Qiao X., Zhang L., Cai S. A photoelectrochemical solar cell based on ZnO/dye/polypyrrole film electrode as photoanode. *Sol. Energ. Mat. Sol. C.*, 2000, **60**, 349-354.

15. Lizama C., Freer J., Baeza J., Mansilla H.D. Optimized photodegradation of Reactive Blue 19 on TiO_2 and ZnO suspensions. *Catal. Today*, 2002, **76**, 235-246.

16. Daneshvar N., Salari D., Khataee A.R. Photocatalytic degradation of azo dye acid red 14 in water on ZnO as an alternative catalyst to TiO_2. *J. Photoch. Photobiol. A*, 2004; 162: 317-322.

17. Akyol A., Yatmaz H.C., Bayramoglu M. Photocatalytic decolorization of Remazol Red RR in aqueous ZnO suspensions. *Appl. Catal. B-Environ.*, 2004, **54**, 19-24.

18. Mrowetz M., Selli E. Photocatalytic degradation of formic and benzoic acids and hydrogen peroxide evolution in TiO_2 and ZnO water suspensions. *J. Photoch. Photobiol. A*, 2006, **108**, 15-22.

19. Peng F., Wang H., Yu H., Chen S. Preparation of aluminum foil-supported nano-sized ZnO thin films and its photocatalytic degradation to phenol under visible light irradiation. *Mater. Res. Bull.*, 2006, **41**, 2123-2129.

20. Kansal S.K., Singh M., Sud D. Studies on photodegradation of two commercial dyes in aqueous phase using different photocatalysts. *J. Hazard. Mater.*, 2007; 141: 581-590.

21. Tan, T.Y.T. *Photocatalytic reduction of selenate and selenite: water/wastewater treatment and the formation of nano-selenium compounds*. Ph. D. Thesis, University of New South Wales, 2003.

22. McKelvey, J.P., *Solid State and Semiconductor Physics*, Happer and Row, New York, 1996.

23. Mori, K., Photo-functionalized materials using nanoparticles: photocatalysis, surface finishing R&D center central research laboratories nihon parkerizing. KONA, 2005, **23**, 205-214.

24. Mills A., Hunte S.L. An overview of semiconductor photocatalysis, *J. Photoch. Photobio. A*., 1997, **108**, 1-35.

25. Liqiang J., Xiaojun S., Jing S., Weimin C., Zili X., Yaoguo D., Honggang F. Review of surface photovoltage spectra of nanosized semiconductor and its applications in heterogeneous photocatalysis. *Sol. Energ. Mat. Sol. C.*, 2003, **79**, 133-151.

26. Liqiang J., Yichun Q., Baiqi W., Shudan L., Baojiang J., Libin Y., Wei F., Honggang F., Jiazhong S. Review of photoluminescence performance of nano-sized semiconductor materials and its relationships with photocatalytic activity. *Sol. Energ. Mat. Sol. C.*, 2006, **90**, 1773-1787.

27. Galindo C., Jacques P., Kalt A. Photodegradation of the aminoazobenzene acid orange 52 by three advanced oxidation processes: UV/H_2O_2, UV/TiO_2 and VIS/TiO_2 Comparative mechanistic and kinetic investigations. *J. Photoch. Photobiol. A,* 2000, **130**, 35-47.

28. Hodnett, B.K., *Heterogeneous Catalytic Oxidation: Fundamental and Technological Aspects of the Selective and Total Oxidation of Organic Compounds*, Department of Chemical and Environmental Sciences and The Materials and Surface Science Institute, University of Limerick, Ireland, 2000.

29. Teoh W.Y., Madler L., Beydoun D., Pratsinis S. E., Amal Rose. Direct (one-step) synthesis of TiO_2 and Pt/TiO_2 nanoparticles for photocatalytic mineralisation of sucrose. *Chem. Eng. Sci.*, 2005, **60**, 5852 – 5861.

30. Liqiang J., Dejun W., Baiqi W., Shudan L., Baifu X., Honggang X., Jiazhong S. Effects of noble metal modification on surface oxygen composition, charge separation and photocatalytic activity of ZnO nanoparticles. *J. Mol. Catal. A: Chem.*, 2006, **244**, 193-200.

31. Sakthivel S., Geissen S.U., Bahnemann D.W., Murugesan V., Vogelpohl A. Enhancement of photocatalytic activity by semiconductor heterojunctions: α-Fe_2O_3, WO_3 and CdS deposited on ZnO. *J. Photoch. Photobiol.* A, 2002, **148**, 283-293.

32. Wang H., Xie C., Zhang W., Cai S., Yang Z., Gui Y. Comparison of dye degradation efficiency using ZnO powders with various size scales. *J. Hazard. Mater.*, 2007, **141**, 645-652.

33. Height M.J., Pratsinis S.E., Mekasuwandumrong O., Praserthdam, P. Ag-ZnO catalysts for UV-photodegradation of methylene blue. *Appl. Catal. B-Environ.*, 2005, **63**, 305-312.